Integration of Self-Assembled Microvascular Networks with Microfabricated PEG-Based Hydrogels

*Michael P. Cuchiara, Daniel J. Gould, Melissa K. McHale, Mary E. Dickinson, and Jennifer L. West**

Despite tremendous efforts, tissue engineered constructs are restricted to thin, simple tissues sustained only by diffusion. The most significant barrier in tissue engineering is insufficient vascularization to deliver nutrients and metabolites during development in vitro and to facilitate rapid vascular integration in vivo. Tissue engineered constructs can be greatly improved by developing perfusable microvascular networks in vitro in order to provide transport that mimics native vascular organization and function. Here a microfluidic hydrogel is integrated with a self-assembling pro-vasculogenic co-culture in a strategy to perfuse microvascular networks in vitro. This approach allows for control over microvascular network self-assembly and employs an anastomotic interface for integration of self-assembled microvascular networks with fabricated microchannels. As a result, transport within the system shifts from simple diffusion to vessel supported convective transport and extra-vessel diffusion, thus improving overall mass transport properties. This work impacts the development of perfusable prevascularized tissues in vitro and ultimately tissue engineering applications in vivo.

1. Introduction

Complex, bulky and metabolically dense engineered tissues require a functional vascular network for survival. Vascularization approaches that rely solely on implant anastomosis with the host are limited by slow host vessel ingrowth (tenths of micrometers per day)[1] and non-homogenous vessel distribution within the construct.[2] The transport regimes that are established result in insufficient delivery of oxygen and nutrients, leading to a necrotic tissue core and a reduction in the overall therapeutic potential of the implant.[3] Engineering microvascular networks *in vitro* prior to implantation, referred to as prevascularization, holds the promise to improve mass transport and rapidly integrate engineered networks with the host tissue upon implantation.[4]

Dr. M. P. Cuchiara, Dr. M. K. McHale
Department of Bioengineering–MS 142
6100 Main St., Houston, TX 77005 USA
Dr. D. J. Gould, Dr. M. E. Dickinson
One Baylor Plaza, Houston, TX 77030 USA
Prof. J. L. West
Department of Bioengineering–MS 142
6100 Main Street, Houston, TX 77005 USA
E-mail: jwest@rice.edu

DOI: 10.1002/adfm.201200976

Prevascularization has been explored in natural[5] and synthetic materials[6] using various cellular components.[7] In one seminal approach, a combination of human umbilical vein endothelial cells (HUVEC) and mesenchymal progenitors (10T1/2) were cultured in a collagen-fibronectin matrix and demonstrated rapid formation of long-lasting, prevascular networks. Of note, the 10T1/2 cells in this co-culture exhibited a pericyte morphology and were deemed necessary for HUVEC tubule stabilization.[8] Despite recent progress in the establishment microvessel-like configurations, no systems have been established to associate and perfuse these self-assembled prevascular networks across clinically relevant length scales *in vitro*. Such advancement would improve *in vitro* mass transport and may facilitate a rapid anastomosis with the host following implantation.[9]

Towards the development of a functional tissue engineered microvasculature, we build upon previous work from our group in which a synthetic, photopolymerizable poly(ethylene glycol) (PEG) hydrogel was shown to support rapid self-assembly of HUVEC and 10T1/2 tubule networks *in vitro*. This pro-vasculogenic hydrogel is fabricated with a PEG-tethered integrin binding peptide (PEG-RGDS) and a proteolytically degradable PEG derivative that incorporates a matrix metalloprotease (MMP)-sensitive peptide sequence within the backbone of the polymer for cell directed degradation of the hydrogel. Cells in these self-assembled prevascular networks replaced the synthetic polymer matrix with the basement membrane proteins, laminin and collagen IV, and the networks remained stable in culture for at least 30 days.[10] We believe that the combination of this synthetic pro-vasculogenic hydrogel with established microfabrication technologies represents an innovative approach to perfuse and integrate self-assembled microvascular networks with nutrient containing microchannels *in vitro*. This integration would allow for controlled convective transport across large length scales and in a wide range of vessel diameters and has the potential to result in improved anastomotic interfaces.

Our strategy to achieve *in vitro* perfusion brings together fabricated hydrogel microchannels (50–1000 μm) with self-assembled microvascular networks (15–50 μm) by combining soft lithographic and photolithographic microfabrication techniques with a pro-vasculogenic PEG hydrogel containing the

HUVEC-10T1/2 co-culture. Hydrogel microchannels provide robust conduits to efficiently deliver and control nutrient and signaling gradients within the construct, while serving as stable anastomotic interfaces for connection to cell tubules. Combining microfabrication and self-assembly techniques bridges macro to micro scale transport, shifts material transport regimes from diffusion through a polymer matrix to vessel supported convection, and allows for biomimetic perfusion of prevascularized constructs *in vitro*.

We report herein that the multilayer, microfluidic, polydimethylsiloxane–poly(ethylene glycol) (PDMS-PEG) hydrogel microdevice we have fabricated can be used to spatiotemporally control microvascular network self-assembly and persistence. In addition, integration of self-assembled microvascular networks with microfabricated channels shifted the biomaterial transport regime to vessel-supported convective transport and subsequent extra-vascular diffusion. This work has direct implications in the development of perfusable pre-vascularized tissues *in vitro* for three dimensional cell culture and regenerative medicine applications.

2. Results and Discussion

2.1. Device Microfabrication

To permit self-assembled microvascular network integration with perfusable microfabricated channels, we developed a dual mode, multilayer, microfabrication strategy to build a microfluidic poly(ethylene glycol) (PEG) hydrogel within a polydimethylsiloxane (PDMS) housing as shown in **Figure 1**. First a transparent PDMS housing with fluid access ports was fabricated using standard soft lithographic techniques. Next, an aqueous solution containing the pro-vasculogenic PEG hydrogel precursors along with a 4:1 mixture of HUVEC and 10T1/2 cells was injected into the PDMS housing. A photomask was used to photolithographically crosslink the cell laden pro-vasculogenic hydrogel in a confined geometry between the perfusion channels. Finally, the PDMS-PEG device was sealed to cover glass and channel perfusion was initiated at flow rates derived from normal physiologic microvascular shear stresses (15 dyne/cm^2) using two syringes pumps.

Hydrogel incorporation within a robust PDMS housing addresses several logistical challenges associated with microfluidic hydrogels without the need for complicated supporting apparatuses.[11] Furthermore, this multilayer approach provides independent control over PDMS housing and PEG hydrogel geometry allowing for freeform user-defined fabrication of tissue-mimetic hydrogel structures within the PDMS housing. A particularly advantageous characteristic of this system is the fabrication of a solution-hydrogel interface between the perfused microchannel and the self-assembled vessel networks within the hydrogel bulk. This interface promotes the connection of fabricated channels with self-assembled vessel structures and facilitates mass transport across large length scales from fabricated channels 1 mm in diameter, a size amenable to surgical anastomosis during implantation, to microvascular networks 30 µm in diameter.

2.2. Evaluation of Self-Assembled Microvascular Networks

The self-assembly of encapsulated cells into vessel-like structures is confirmed by the confocal image in **Figure 2**. Here we note that HUVECs (green, fluorescent anti-PECAM) arrange in tubule networks that are stabilized on their external surface by pericyte-functioning 10T1/2 cells (red, fluorescent anti-smooth muscle α-actin). In order to promote spatially homogeneous microvascular network formation within the device, it is advantageous to maximize this network self-assembly as a function of distance from the perfused channel. Though the inclusion of microfluidic channels within engineered tissue constructs has been shown to improve mass transport and increase cell viability,[12] the fraction of viable cells decreases significantly with increasing distance from the media-perfused conduit.[6,7] Formation and perfusion of 3D,

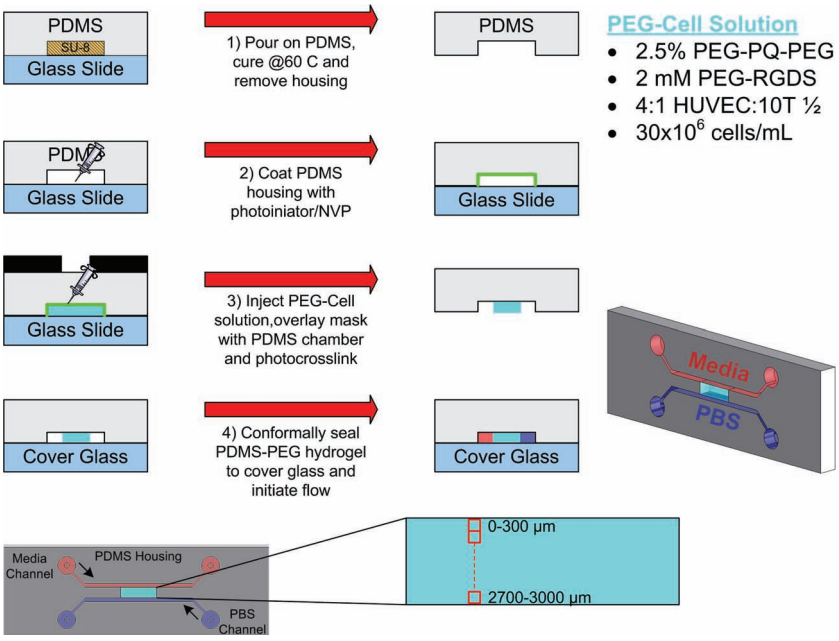

Figure 1. Microfabrication system design schematic. PDMS is replica molded to fabricate an external perfusion housing (Step 1). The interior of the housing is coated with photoinitiator (Step 2), and then photopolymerizable PEG precursors are injected into the housing and mask directed photolithography is used to fabricate hydrogel microchannels within the external PDMS housing (Step 3). The PDMS–PEG multilayer device is conformally sealed to coverglass and perfused with media and buffer (Step 4). The final schematic shows the spatial relationship of the perfused media (red) and buffer (blue) microchannels to PEG hydrogel (cyan) regions imaged for analysis in this study.

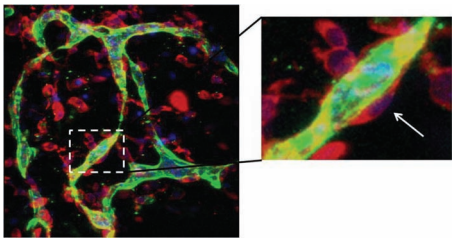

Figure 2. Microvascular network formation. In this representative immunohistochemistry (IHC) image of the microvasculature at 96 h in the region 0–300 μm from the media microchannel, HUVECs (green; anti-PECAM) are shown forming connected networks with 10T1/2 cells (red; anti-smooth muscle α-actin) acting as pericytes to wrap and therefore stabilize vessel networks (inset; arrow). Cell nuclei appear blue with DAPI counterstaining. Dimensions of the field of view (FOV) for the large image are 318 μm × 318 μm with an inset FOV of 76 μm × 57 μm.

self-assembled microvascular networks between fabricated microchannels shifts the characteristic diffusion length from the process limited channel spacing[13] to the shorter distance arising between self-assembled vessels formed from the co-culture.

We set out to determine the maximum distance from a perfused media channel that supports microvascular network self-assembly and cell survival in the pro-vasculogenic PEG hydrogel. For this study, dually-perfused microchannel devices were operated in either a Media-Buffer configuration, roughly analogous to capillary-lymphatic mass exchange, or a Media-Media configuration, more similar to inter-capillary transport. Spatiotemporal vessel formation was evaluated by morphological assessment of the number of tubules, as well as total tubule lengths and immunohistochemical analysis with an antibody to the endothelial membrane marker PECAM. An apoptotic assay was conducted concurrently to determine the relationship between microchannel configurations and cell viability.

2.2.1. Microvessel Network Morphology is Influenced by Distance from Perfused Nutrients

Self-assembly of HUVEC and 10T1/2 cells into microvascular networks in the Media-Buffer configuration was highly dependent upon culture time and distance from the microchannel. A trend of decreasing total tubule length and total tubule number with increasing distance from the nutrient source was observed at both 48 h and 96 h of culture (**Figure 3**a,b and **Figure 4**a,b). Both total tubule length and total tubule number at 96 h were significantly greater in the nutrient rich regions (<600 μm from the media microchannel) when compared to regions greater than 600 μm ($p < 0.05$, $n = 3$, Figure 4a,b). However, this trend was not evident at early time points in microvascular network formation, where initial vessel coalescence and self-assembly were relatively homogeneous (Figures 3 and 4; t = 48 h). Moreover, only those regions closest to the media source (0–300 μm from microchannel) experienced significant increases in total tubule number and length from 48 h to 96 h ($p < 0.05$, $n = 3$, Figures 3 and 4), while at the interior (900–2100 μm) there were a significant decreases in the number and length of tubules over the same time period ($p < 0.05$, $n = 3$, Figures 3 and 4).

The Media-Media configuration encouraged the establishment of vessel networks at distances farther from the microchannel than in the Media-Buffer configuration, displaying high levels of self-assembly throughout the entire thickness of the hydrogel at 96 h (Figure 4a,b, hashed bars). Perhaps the most interesting characteristic of the Media-Media configuration is its ability to support robust microvascular network growth from 48–96 h. In these microfluidic devices, all regions experienced increases in tubule length and number from 48–96 h, whereas in the Media-Buffer system this increase was only evident in regions less than 300 μm from the media channel.

2.2.2. Spatiotemporal Assessment of Cell Apoptosis

The lack of robust microvascular network self-assembly in regions farthest from the perfused media microchannel was thought to be due to apoptosis driven by nutrient deprivation. A spatiotemporal TUNEL assay was applied to the Media-Buffer system at 48 h and 96 h and apoptotic activity within the construct was shown to be inversely related to microvascular network self-assembly. At 96 h of culture, the region nearest the media microchannel (**Figure 5**; 0–300 μm) had a significantly lower fraction of TUNEL positive cells ($p < 0.05$, $n = 3$).

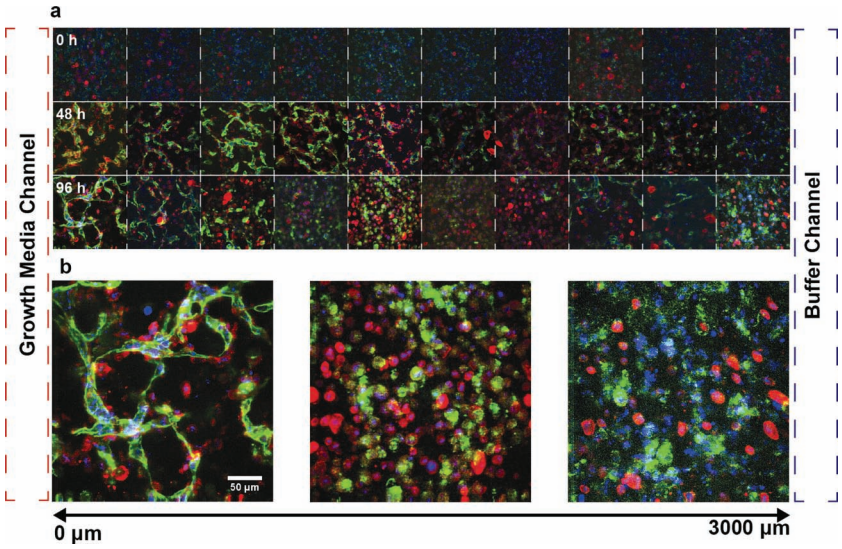

Figure 3. Spatiotemporal microvascular network morphology. (a) Immunohistochemistry fluorescent micrographs of HUVECs (green; anti-PECAM), 10T1/2 (red; anti-smooth muscle α-actin) and DAPI (blue) as a function of culture time (0, 48, and 96 h) and distance (0–3000 μm) from the perfused media microchannel. Co-cultures begin as homogeneously dispersed 3D suspensions (0 h) and self organize to form tubules over 96 h. The distance between dotted lines is 318 μm. (b) Enlarged images of the 0-300 (left) 1200–1500 (center) and 2700–3000 μm (right) regions at 96 h.

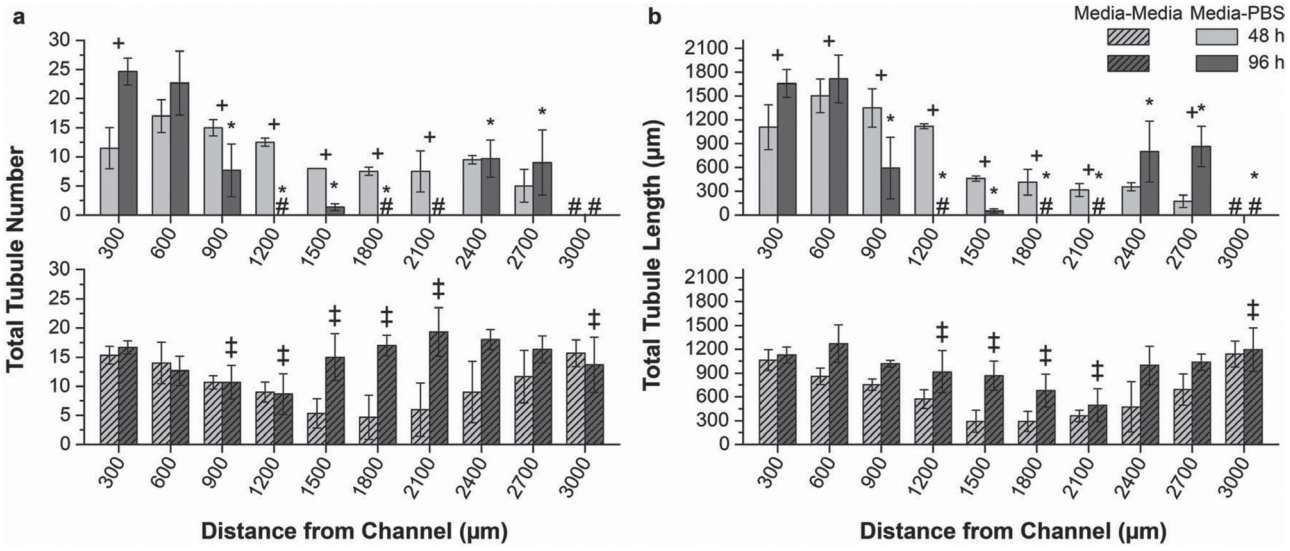

Figure 4. Spatiotemporal self-assembled microvascular network morphology. Total tubule number (a) and total tubule length (b) in a Media-Buffer configuration (solid bars) and a Media-Media configuration (hashed bars) as a function of distance from the microchannel (0–3000 μm) and perfusion time (48 h and 96 h). Robust microvascular network formation in the Media-Buffer system was confined to regions closest to the media microchannel (0–600 μm) with the interior regions (1200–2100 μm) not forming networks at 96 h. The Media-Media configuration permitted microvascular network formation farther from the microchannel but with an overall lower number of total tubules and a decrease in total tubule length at each time and location when compared to the Media-Buffer configuration. $p < 0.05$, $n = 3$, paired t-test, (+) indicates 48 h vs. 96 h temporal significance, (*) indicates spatial significance compared to the 0–300 μm region, and ‡ indicates significance between Media-Media and Media-Buffer at 96 h.

Furthermore the apoptotic fraction increased from 48 h to 96 h in the same regions where total tubule length and number were shown to decrease. Interestingly the nutrient rich region (0-300 μm) that experienced increases in total tubule number and length from 48 h to 96 h also exhibited low but significant increases in apoptotic activity over the same time period. This upregulation of programmed cell death is likely due to tubule pruning that is characteristic of maturing microvascular networks.[14] These observations taken together are suggestive of initially high and homogeneous self-assembly into a nascent capillary plexus from 0–48 h, followed by network maturation in the nutrient rich regions and network regression in apoptotic regions from 48–96 h.

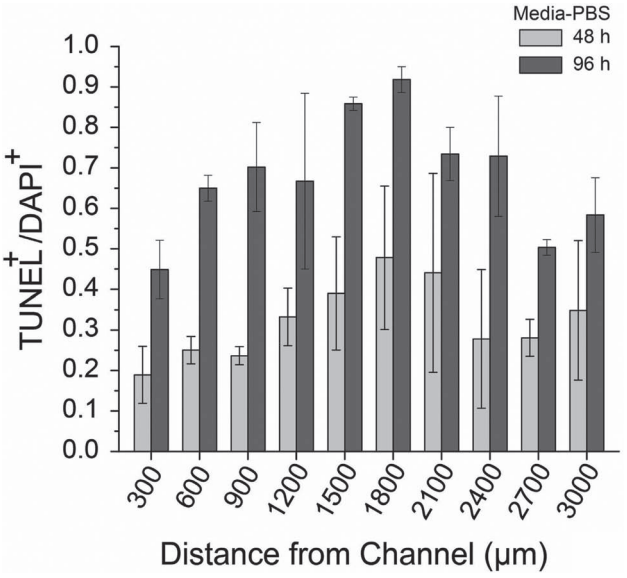

Figure 5. Spatiotemporal apoptotic activity. Spatiotemporal apoptotic activity was assessed using the TUNEL marker for damaged DNA. After 96 h of culture, the region nearest the media microchannel (0–300 μm) had a significantly lower fraction of TUNEL positive cells. Furthermore the TUNEL positive fraction was shown to increase from 48 h to 96 h in the same regions where total tubule length and number were shown to decrease.

2.3. Discerning Transport Modes in Vascularized and Non-Vascularized Hydrogels

The vasculature provides mass transport over large distances in the body *via* rapid, lumen-supported convection followed by diffusion out of the microvascular networks and into the tissues.[15,16] *In vitro* integration of self-assembled microvascular networks and perfusion with fabricated channels recapitulates *in vivo* network hierarchies and promotes efficient, biomimetic mass transport regimes with the potential to yield more clinically relevant engineered tissues. In validating the effectiveness of our microfluidic system, we compared the mass transport characteristics between vascularized and non-vascularized hydrogels. Pro-vasculogenic PEG hydrogels containing the co-culture of HUVEC and 10T1/2 cells were perfused in the Media-Media configuration for 96 h to drive microvascular network self-assembly and integration with fabricated microchannels. After 96 h of culture, growth medium was supplemented with high molecular weight fluorescent dextran (2×10^6 Da, lysine fixable) and time-lapse confocal microscopy was used to image

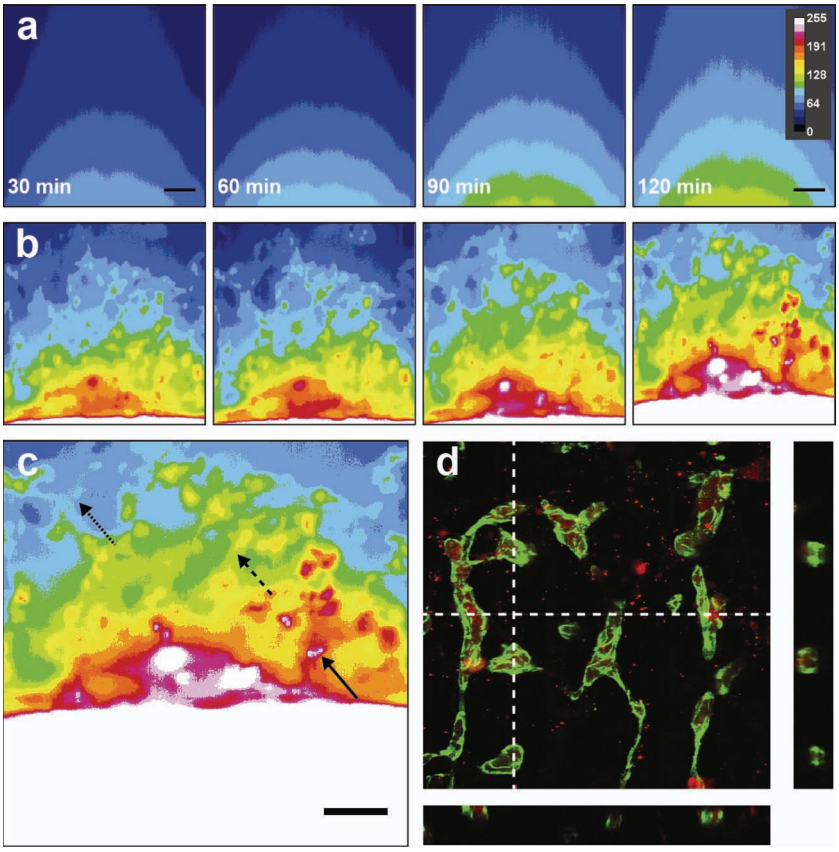

Figure 6. Mass transport regimes in vascularized and non-vascularized PEG scaffolds. (a) Time-lapse high molecular weight dextran intensity maps of regions directly adjacent to the microchannel wall. Non-vascularized transport profiles behave according to Fickian diffusion through a polymer matrix. (b) Time-lapse high molecular weight dextran intensity maps of regions directly adjacent to the microchannel wall in vascularized scaffolds at 96 h of culture. Rapid convective like transport through the matrix in regions coinciding with vessel structures suggests a shift in transport from diffusional transport to convection through vessel structures. (c) Enlarged high molecular weight dextran intensity map at 120 min post perfusion. Dotted arrows indicate newly perfused vessels, dashed and solid arrows indicate progressively broadening intensity profiles suggesting extra-vessel diffusion. (d) Confocal z-stack and orthogonal projection of fixed high molecular weight dextran (red) and anti-PECAM IHC (green) in vascularized scaffolds at 96 h of culture. Dextran co-localization within PECAM labeled vessel lumen suggests transport via vessel structures. Scale bars in (a) and (c) are 50 µm, FOV for the primary image in (d) is 318 µm.

transport through the vascularized construct for 180 minutes. Non-vascularized controls were fabricated identically but without the inclusion of cells. Dextran accumulation and the spatiotemporal fluorescence intensity landscape in the region adjacent to the perfused microchannels were compared between the two systems.

Though encapsulated cells in vascularized hydrogels have the capacity to alter the diffusive properties of the material via polymer degradation or extracellular matrix (ECM) deposition during long term culture, our observations suggest that the vascularized system supports enhanced mass transport characterized by combined convection and diffusion. Non-vascularized hydrogels exhibited a uniformly advancing dextran intensity front characteristic of 1D Non-Steady State Fickian diffusion of a solute through a hydrogel matrix (**Figure 6**a and **Figure 7**a),[12,17,18] while vascularized hydrogels displayed rapid, convective-like dextran transport in regions spatially coinciding with vessel structures (Figure 6b, c, and d). At each time point, fluorescent dextran can be seen at greater distances from the perfused microchannel in the vascularized construct when compared to the non-vascularized construct (Figure 6a and b, and 7a). Accordingly, at a fixed distance from the microchannel, the rate of dextran accumulation in the vascularized system was significantly greater than the non-vascularized system during the first 30 minutes of perfusion ($p < 0.05$, $n = 9$, Figure 7b). Interestingly, this difference in movement in the vascularized and non-vascularized hydrogels (Figure 7b,% Convective Transport) is most extreme at early time points when convection is dominant and decreases over time as system transport becomes diffusion limited.

Spatially, we observed rapid intensity increases in dextran distribution in the vascularized system occurring ahead of the diffusion front, indicative of convective, vessel-supported transport. Examples of this occurrence are highlighted by the arrows in Figure 6c, and are also visible in Figure 7a. This observation suggests a shift in transport regimes from Fickian diffusion to rapid lumen-supported convection through the vessel networks. To further validate that microvascular lumen supported convective transport, dextran perfused vascularized constructs were fixed and immunohistochemically evaluated for the endothelial marker PECAM to determine the proximity of perfused dextran to vessel lumen. Confocal imaging showed perfused dextran predominantly co-localized with the lumen of microvascular structures, further demonstrating transport via the newly formed vessels (Figure 6d).

In addition to supporting convective transport, vascularized constructs displayed a greatly reduced characteristic diffusion length ($\lambda_V = 67$ µm) when compared to the acellular system ($\lambda_D = 3$ mm). Diffusion lengths in the vascularized hydrogel are defined by vessel density and spacing, not overall construct geometry (Figure 7a). This significant reduction in required solute travel highlights an important shift towards a biomimetic transport regime wherein characteristic diffusion lengths are less than the critical necrotic distances. Time lapse dextran intensity profiles also show broadening of profile intensities and a decrease in peak intensity aspect ratio over time (Figure 6b and Figure 7c and d). Together these observations suggest vascularized constructs support initial convective-like transport and extra-vessel diffusion into the interstitial space, recapitulating the functional properties of the microvasculature.

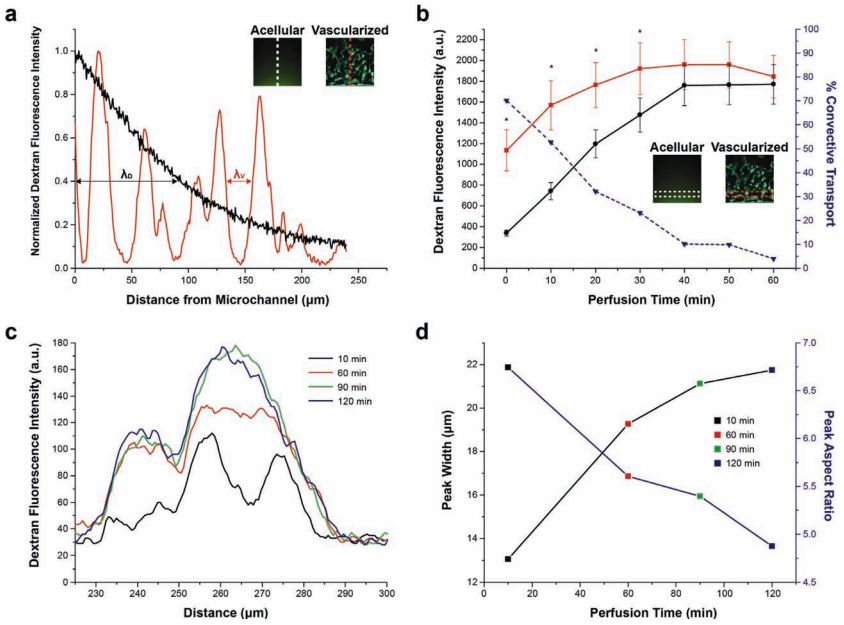

Figure 7. Vascularization effects on mass transport. (a) High molecular weight dextran intensity profiles in non-vascularized (black trace) and vascularized (red trace) hydrogels. Non-vascularized hydrogels rely on diffusional transport with construct characteristic diffusion lengths (λ_D) limited to large distances between perfused microchannels. Vascularized hydrogels exhibit convective transport that rapidly penetrates hundreds of micrometers into the hydrogel with characteristic diffusion lengths (λ_V) limited to the small distance between vessels. (b) At early time points when convection dominates, high molecular weight dextran accumulates at a significantly greater rate in the vascularized system (red trace) when compared to the non-vascularized system (black trace) ($p < 0.01$, $n = 5$, paired t-test). The difference in vascularized and non-vascularized transport or the % convective transport shown as a percentage of total intensity (blue dash trace) is greatest at early time points and decreases as transport becomes diffusion limited. (c) Time-lapse (0-120 min) high molecular weight dextran intensity profiles in the vascularized constructs show diffusion out of vessel structures as indicated by (d) peak width broadening and a decrease in peak aspect ratio over time. FOVs for the inset images are 318 μm.

3. Conclusions

In conclusion, we report the combination of robust microfabrication technologies with a pro-vasculogenic, synthetic hydrogel and an endothelial cell/pericyte precursor co-culture that enables the perfusion of self-assembled microvascular networks within a multilayer microfluidic device. Spatiotemporal characterization of microvascular network self-assembly allowed for the determination of optimal microchannel spacing that promotes homogeneous microvascular network formation. Perhaps the most significant finding relating to the development of vascularized engineered tissues is the shift in mass transport regimes from strict diffusion through the hydrogel matrix to microvasculature network supported convection followed by extra-vessel diffusion. Anastomotic integration of externally fabricated synthetic structures with cell-generated microvascular networks enables this shift and provides a valuable tool towards the recapitulation of vascular hierarchies across multiple tissue length scales. This system has applicability in the development of improved preclinical tissue models and more clinically relevant, pre-vascularized tissue engineered therapeutics.

4. Experimental Section

Cell Maintenance: Human umbilical vein endothelial cells (HUVECs) (Lonza, Walkersville, MD) were cultured in endothelial growth medium (EGM-2, Lonza) supplemented with 2 mM L-glutamine, 1000 U mL^{-1} penicillin, and 100 mg L^{-1} streptomycin (Sigma-Aldrich, St. Louis, MO) and used from passages 3–8. 10T1/2 cells (American Type Culture Collection, Rockville, MD) were maintained in Dulbecco's Modified Eagle's Medium (DMEM) supplemented with 10% fetal bovine serum (FBS), 2 mM L-glutamine, 1000 U mL^{-1} penicillin, and 100 mg L^{-1} streptomycin (Sigma-Aldrich) and used from passages 16-20. All cells were incubated at 37 °C in a 5% CO_2 environment.

Proteolytically Degradable PEG Pre-Polymer Synthesis: Extracellular matrix (ECM) derived peptide sequences have been shown to be specifically cleaved by matrix metalloproteases (MMPs) secreted by tissue cells.[19] Incorporation of the collagen mimetic peptide sequence (GGPQGIWGQGK) into materials based on non-proteolytically degradable synthetic polymers has been shown to result in complete degradation of the polymer network by specific MMPs as well as other broad acting proteases.[10] Furthermore, the conjugation of the GGPQGIWGQGK sequence to monoacrylate, photocrosslinkable PEG macromers in an ABA block co-polymer configuration has demonstrated the ability to promote hydrogel remodeling and support microvascular network formation by HUVECs and 10T1/2 co-cultures.[10]

The peptide sequence GGPQGIWGQGK was generated by standard solid phase FMOC chemistry using an Apex396 peptide synthesizer (Aapptec, Louisville, KY). Following synthesis and purification, the peptide product was verified by matrix-assisted laser desorption ionization time of flight mass spectrometry (MALDI-ToF; Bruker Daltonics, Billerica, MA). A diacrylate ABA block co-polymer of the peptide sequence was synthesized by reacting heterobifunctional acrylate-PEG-succinimidyl carboxymethyl (Laysan Bio, Arab, AL; acrylate-PEG-SCM, 3400 Da) in a 1:2.2 (peptide:PEG) molar ratio in anhydrous dimethylsulfoxide (DMSO, Sigma-Aldrich) in the presence of 15 mM N,N-Diisopropylethylamine (DIPEA, Sigma-Aldrich) overnight. This reaction conjugates PEG monoacrylates to both the amine terminus of the peptide sequence and to the lysine amino side-chain at the peptide carboxy terminus using standard succinimide-amine chemistry. The resulting reaction volume was slowly diluted 2:1 in an ice bath with ultrapure H_2O and dialyzed (5000 MWCO regenerated cellulose, Spectrum Laboratories, Rancho Dominguez, CA) against ultrapure H_2O for 48 h to remove DIPEA, DMSO, and un-reacted PEG and peptide moieties. The product was then frozen at –80 °C, lyophilized for 72 h and stored under argon at –80 °C until further use. The cell adhesive ligand Arg-Gly-Asp-Ser, (RGDS, American Peptide Sunnyvale, CA) was conjugated to acrylate-PEG-SCM in a 1:1.1 (PEG:RGDS) molar ratio under the same conditions as the PEG-Peptide-PEG block co-polymer. Successful polymer conjugations were confirmed via gel permeation chromatography with UV-vis and evaporative light scattering detectors (Polymer Laboratories, Amherst, MA).

Multilayer Photolithographic Fabrication of Perfused PEG Scaffold: Poly(dimethylsiloxane) (PDMS, Sylgard 184) housings were prepared using standard soft lithographic techniques as previously described.[12] Briefly, PDMS (15:1, silicone elastomer: curing agent) was molded to photoresist masters (SU-8 2100, 350 μm in height, Microchem, Newton, MA) to create a robust housing with perfusion access ports and transparent optical qualities for ease of imaging (Figure 1). All

PDMS surfaces were treated with the photoinitiator acetophenone (2,2-dimethoxy-2-phenyl acetophenone in *n*-vinylpyrrolidone, 300 mg mL^{-1}, Sigma) for 5 min to promote free radical induced interfacial polymerization of the acrylate terminated PEG pre-polymer solution to the housing. Excess photoinitiator was removed via sequential rinsing with 100% ethanol and ultrapure H_2O, which was followed by drying with filtered air. Acetophenone-coated PDMS housings were sealed to glass slides treated with SigmaCote (Sigma-Aldrich, St. Louis, MO) and overlaid with a transparency photomask (20,000 dpi, CAD/ART Services, Bandon, OR) aligned to control spatial photopolymerization and hydrogel geometry within the PDMS (Figure 1).

The MMP-degradable PEG block copolymer and PEG-RGDS cell-adhesive derivative were dissolved in EGM-2 to final concentrations of 2.5% (w/v) and 2 mM, respectively. The photoinitiator Irgracure-2959 (Ciba, 100 mg mL^{-1} in 200 proof ethanol) was added to the pre-polymer solution at 30 μL mL^{-1}. HUVECs and 10T1/2 cells were suspended in the pre-polymer solution in a 4:1 ratio (HUVEC:10T1/2) to a final concentration of 30×10^6 cell mL^{-1}. The resulting cell/pre-polymer solution was injected into the PDMS housing via the perfusion access ports and exposed through the photomask to long wavelength UV light (365 nm, 10 mW cm^{-2}) for 5 min to fabricate the PEG hydrogel structures. The PDMS housing with the embedded photocrosslinked PEG hydrogel was gently rinsed with sterile phosphate buffered saline (PBS, pH 7.4), dried with canned air and sealed to #1 cover glass. The cell/hydrogel construct was perfused at 600 μL h^{-1} with EGM-2 at one interface and sterile PBS on the opposite interface to establish a gradient of growth factors, nutrients, and waste species across the construct (Media-Buffer configuration, Figure 1). Some experiments were conducted in a Media–Media configuration in which both hydrogel construct channel interfaces were perfused with EGM-2 in order to determine the maximum distance microvascular networks would develop from the perfused nutrient source.

Immunohistochemistry: Immunofluorescence analysis was performed to determine spatiotemporal microvascular network characteristics and the cell-cell relationships within the co-culture. At 0, 48 and 96 h perfusion was terminated and hydrogel microdevices were fixed, permeabilized, and reacted with primary and secondary antibodies (Figure 2). The primary antibodies used were mouse anti-smooth muscle α-actin (Sigma-Aldrich) to label the 10T1/2 cells and goat anti-PECAM (Santa Cruz Biotechnology, Santa Cruz, CA) to label membranes of HUVECs. The secondary antibodies were anti-mouse and anti-goat conjugated with either Alexa fluor 488, Alexa fluor 532, or Alexa fluor 647. DAPI (300 nM, Invitrogen) was added as a nuclei counter stain for all immunofluorescence images.

Spatiotemporal Microvascular Network Morphology Analysis: Spatiotemporal PECAM immunofluorescence images were analyzed at 0, 48 and 96 h post device fabrication to determine the effects of perfusion time and distance from the EGM-2 perfused microchannel on microvascular network morphology (Figure 3a and 3b). The PECAM immunofluorescence was imaged using a confocal microscope (Zeiss LSM 5 Live, 20x/NA 0.8 objective, FOV 318 × 318 μm, vertical z-stack: 1 μm slices, 50 slices per region, Carl Zeiss Inc., Thornwood, NY). Image regions were tiled at 300 μm intervals radially outward from the perfused media microchannel wall to the PBS microchannel wall for a total of 10 regions spanning the 3 mm thickness of the hydrogel construct.

Pre-processing of the LSM images was accomplished by first applying a maximum intensity projection to the z-stack using the image browser function in the LSM Image Examiner software (Carl Zeiss Inc., Thornwood, NY). After maximum intensity projection, channels were split and the PECAM immunofluorescence channel was thresholded to preserve the tubule elements, while decreasing the background signal. The resulting thresholded image was then used to measure the lengths of the tubule elements within the construct. Each tubule was measured manually using the image browser measurement tool, where single tubules were determined as starting at one branch and ending at another. Both the tubule lengths and the total tubule number were recorded for each image at different locations within the constructs.

Spatiotemporal TUNEL Apoptosis Assay: Spatiotemporal apoptotic profiles at 48 h and 96 h of culture were analyzed using the Click-It TUNEL assay for DNA fragmentation (Invitrogen, Carlsbad, CA). Samples were fixed, permeabilized, and labeled according to manufacturer recommended protocols and counterstained with DAPI (300 nM, Invitrogen). Fragmented DNA fluorescence was imaged using a confocal microscope (Zeiss LSM 5 Live, 20x/NA 0.8 objective, FOV 318 × 318 μm, vertical z-stack: 1 μm slices, 50 slices per region). Again image regions were tiled at 300 μm intervals radially outward from the perfused media microchannel wall to the PBS microchannel wall for a total of 10 regions spanning the 3 mm thickness of the hydrogel construct. At each region and time point, the ratio of apoptotic cells (TUNEL positive) to total cells (DAPI positive) was analyzed and plotted to indicate percentage of apoptotic cells. Control samples treated with 70% ethanol were used to set the TUNEL positive imaging parameter values and to avoid false positive TUNEL signal.

Analysis of Acellular and Vascularized Mass Transport: System mass transport properties were analyzed in vascularized and acellular PEG hydrogel constructs after 96 h of culture. High molecular weight fluorescent dextran (dextran- FITC, lysine fixable, 2×10^6 Da; Invitrogen, Carlsbad, CA) was added to the perfusion media and flow was set at 600 μL h^{-1}. Images of the region immediately adjacent to the microchannel wall were collected for 120 min via time lapse live-cell fluorescent confocal microscopy (Figure 4a, 4b, and 4c) (Zeiss LSM 5 Live, 20x/NA 0.8 objective, FOV 318 × 318 μm, vertical z-stack: 10 μm slices, 6 slices per region). Following time lapse imaging, a subset of vascularized hydrogels was fixed using 4% paraformaldehyde and then reacted with the PECAM antibody and DAPI nuclear counterstain to determine the spatial localization of dextran relative to vessel structures (Figure 4d).

Differences in the dextran fluorescent intensity landscape of the acellular and vascularized images were assessed using the Plot Profile function in Image J (NIH, Bethesda, MD). Raw intensity values were normalized to maximum intensity in order spatially overlay the data (Figure 5a). As shown in Figure 5b, the rates of dextran transport in the acellular and vascularized systems were assessed by measuring the total fluorescence intensity in a region 50 μm from the channel wall over time using the Image Processing Toolbox in MatLab (Mathworks, Natick, MA). The difference in vascularized and acellular dextran accumulation (Figure 5b,% Convective Transport, blue trace) was determined by taking the difference of vascularized and acellular values at a time point and plotting as a percentage of the vascularized value as in Equation 1. To evaluate extra-vessel diffusion, changes in vascularized intensity peak widths and peak aspect ratios (Equation 2) were measured over time at a constant intensity value with the results plotted in Figure 5c and 5d.

$$\%Convective\ Transport = \frac{Vascularized\ Intensity_t - Acellular\ Intensity_t}{Vascularized\ Intensity_t} \times 100 \quad (1)$$

Equation 1: Equation for calculation of % convection transport trace.

$$Aspect\ Ratio = \frac{Peak\ Height}{Peak\ Width} \quad (2)$$

Equation 2: Calculation of peak aspect ratio.

Received: April 5, 2012
Published online: June 20, 2012

[1] E. R. Clark, E. L. Clark, *Am. J. Anat.* **1939**, *64*, 251–301.
[2] P. Carmeliet, R. K. Jain, *Nature* **2000**, *407*, 249–257.
[3] J. Malda, J. Rouwkema, D. E. Martens, E. P. Le Comte, F. K. Kooy, J. Tramper, C. A. van Blitterswijk, J. Riesle, *Biotechnol. Bioeng.* **2004**, *86*, 9–18.
[4] J. Rouwkema, N. C. Rivron, C. A. van Blitterswijk, *Trends Biotechnol.* **2008**, *26*, 434–441.

[5] R. F. Nicosia, A. Ottinetti, *In Vitro Cell Dev Biol.* **1990**, *26*, 119–128.
[6] M. C. Ford, J. P. Bertram, S. R. Hynes, M. Michaud, Q. Li, M. Young, S. S. Segal, J. A. Madri, E. B. Lavik, *Proc. Nat. Acad. Sci. USA* **2006**, *103*, 2512–2517.
[7] O. Tsigkou, I. Pomerantseva, J. A. Spencer, P. A. Redondo, A. R. Hart, E. O'Doherty, Y. Lin, C. C. Friedrich, L. Daheron, C. P. Lin, C. A. Sundback, J. P. Vacanti, C. Neville, *Proc. Natl. Acad. Sci. USA* **2010**, *107*, 3311–3316.
[8] N. Koike, D. Fukumura, O. Gralla, P. Au, J. S. Schechner, R. K. Jain, *Nature* **2004**, *428*, 138–139.
[9] L. G. Griffith, M. A. Swartz, *Nat. Rev. Mol Cell Biol.* **2006**, *7*, 211–224.
[10] J. J. Moon, J. E. Saik, R. A. Poché, J. E. Leslie-Barbick, S. H. Lee, A. A. Smith, M. E. Dickinson, J. L. West, *Biomaterials* **2010**, *31*, 3840–3847.
[11] N. W. Choi, M. Cabodi, B. Held, J. P. Gleghorn, L. J. Bonassar, A. D. Stroock, *Nat. Mater.* **2007**, *6*, 908–915.
[12] M. P. Cuchiara, A. C. B. Allen, T. M. Chen, J. S. Miller, J. L. West, *Biomaterials* **2010**, *31*, 5491–5497.
[13] C. J. Bettinger, E. J. Weinberg, K. M. Kulig, J. P. Vacanti, Y. Wang, J. T. Borenstein, R. Langer, *Adv. Mater.* **2005**, *18*, 165–169.
[14] R. K. Jain, *Nat. Med.* **2003**, *9*, 685–693.
[15] A. C. Guyton, J. E. Hall, *Textbook of Medical Physiology*, 10th ed. Saunders, Philadelphia **2000**.
[16] L. E. Gerlowski, R. K. Jain, *Microvas. Res.* **1986**, *31*, 288–305.
[17] Y. Ling, J. Rubin, Y. Deng, C. Huang, U. Demirci, J. M. Karpae, A. Khademhosseini, *Lab Chip* **2007**, *7*, 756–762.
[18] N. W. Choi, M. Cabodi, B. Held, J. P. Gleghorn, L. J. Bonassar, A. D. Stroock, *Nat. Mater.* **2007**, *6*, 908–915.
[19] V. Imper, H. E. Van Wart, in *Matrix Metalloproteinases*. (Eds.: R. P. Mecham, W. C. Parks), Academic Press, San Diego **1998**, pp. 219–240.